Hyperspectral Vegetation Indices

3 authors:

Dar A. Roberts
University of California, Santa Barbara
407 PUBLICATIONS   22,480 CITATIONS

SEE PROFILE

Keely Roth
University of California, Davis
23 PUBLICATIONS   574 CITATIONS

SEE PROFILE

Ryan L. Perroy
University of Hawaiʻi at Hilo
19 PUBLICATIONS   434 CITATIONS

SEE PROFILE

Some of the authors of this publication are also working on these related projects:

Project   Three decades of anthropogenic fire activity in a Neotropical agricultural frontier   View project

Project   Selection of HyspIRI optimal band positions for the earth compositional mapping using HyTES data   View project

14 Hyperspectral Vegetation Indices

Dar A. Roberts[1], Keely L. Roth[2], Ryan L. Perroy[3]

1. Department of Geography, EH 1832, University of California, Santa Barbara, CA 93106, USA, Email: dar@geog.ucsb.edu, Tel: 805-308-2838
2. Department of Geography, EH 1832, University of California, Santa Barbara, CA 93106, USA, Email: klroth@geog.ucsb.edu, Tel: 805-893-4434
3. Department of Geography and Earth Science, University of Wisconsin-La Crosse, 1725 State St., La Crosse WI, 54601, Email: perroy.ryan@uwlax.edu, Tel: 608-785-8334.

CONTENTS

14.1 Introduction

Vegetation properties are often measured by converting a reflectance spectrum into a single number value or Vegetation Index (VI). Hyperspectral, or Narrow-band [1], Vegetation Indices (HVIs) include narrower band features or wavelengths only captured by hyperspectral instruments (e.g. [2]). Vegetation properties measured with HVIs can be divided into three main categories: 1) Structure; 2) Biochemistry and; 3) Plant physiology/stress. Measured structural

properties include fractional cover, green leaf biomass, Leaf Area Index (LAI), senesced

biomass, and Fraction Absorbed Photosynthetically Active Radiation (FPAR) [3-5]. A majority

of the indices developed for structural analysis were formulated for broad band systems and have

Narrow-band, hyperspectral equivalents. Biochemical properties include water, pigments

(chlorophyll, carotenoids, anthocyanins), other nitrogen-rich compounds (e.g. proteins) and plant

structural materials (lignin and cellulose) [6-8]. Physiological and stress indices measure subtle

changes due to a stress-induced change in the state of xanthophylls [9], changes in chlorophyll

content [10], fluorescence [11] or changes in leaf moisture [12]. In general, biochemical and

physiological/stress indices were formulated using laboratory or field instruments (<= 10 nm

spectral sampling) and are targeted at very fine spectral features. As a result they are strictly

hyperspectral. The one exception is indices developed for water.

Many structurally-oriented VIs rely on some combination of Near-Infrared (NIR) to red

reflectance, such as the NIR to red ratio, or Simple Ratio (SR:[3]). This is because increases in

LAI correspond with increases in chlorophyll absorption and NIR-scattering and decreases in

exposed substrate, resulting in decreasing red and increasing NIR reflectance (Figure 14.1).

Thus, equations for these VIs often compare reflectance at an absorbing wavelength to a non-

absorbing wavelength. However, more subtle changes also occur with an increase in LAI,

including increasing green reflectance [13] and increases in the absorption of liquid water [14].
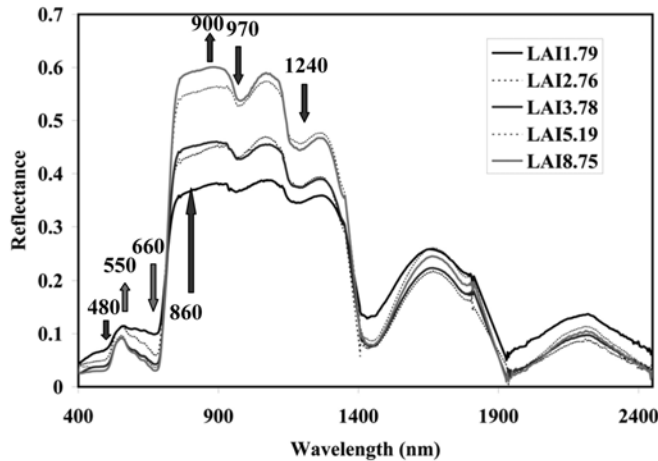
Figure 14.1 Reflectance spectra of *Populus trichocarpa* hybrids over a range in Leaf Area Index. Wavelengths labeled refer to absorption features (480, 660, 970, 1240 nm) or NIR scattering regions (860, 900 nm) typically used in combination to quantify structure. Arrows mark regions of decreasing reflectance due to absorption (down) or increasing reflectance due to scattering (up).

Biochemical and stress-related indices rely on a similar comparison of absorbing and non-absorbing wavelengths, varying the absorbing wavelength by biochemical (Figure 14.2). For example, canopy moisture/moisture stress indices include wavelengths associated with liquid water absorption (e.g. 970, 1200 nm), while ligno-cellulose content indices utilize the Short-Wave-Infrared (SWIR) and wavelengths from 1500 to 1800 nm and 2000 to 2350 nm (Figure 14.2). By contrast, pigments (carotenoids, anthocyanins and chlorophylls) absorb in the visible and ultraviolet, with distinct, but overlapping absorption features. Chlorophyll primarily absorbs blue and red light (*AcerLf*, Figure 14.2). Anthocyanins absorb all but red light (*Fagus*, Figure 14.2); and many carotenoids are yellow due to strong blue light absorption (*Betula*, Figure 14.2). Thus, pigment-sensitive VIs frequently include a combination of visible bands.
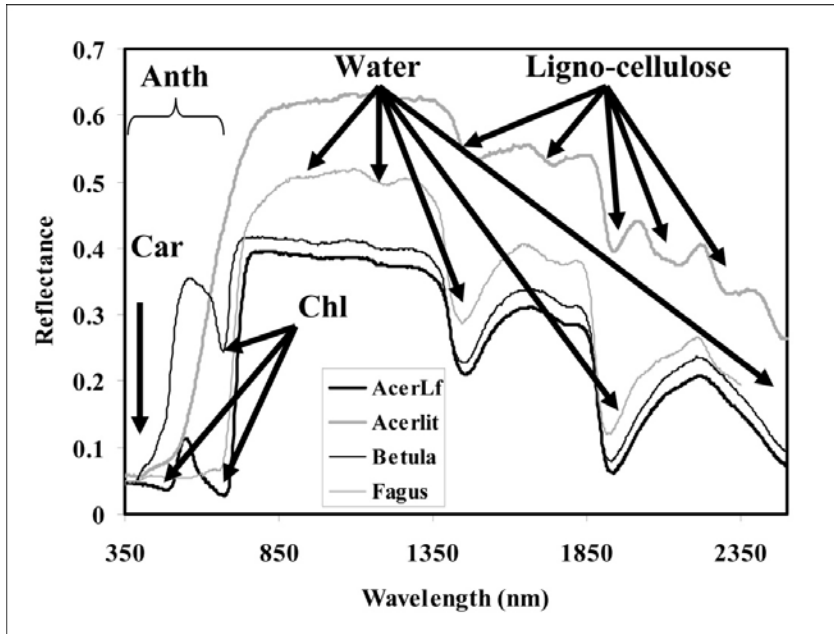
Figure 14.2 Reflectance spectra of leaves from a senesced birch (Betula), ornamental beech (Fagus) and healthy and fully senesced maple (AcerLf, Acerlit) illustrating Carotenoid (Car), Anthocyanin (Anth), Chlorophyll (Chl), Water and Ligno-cellulose absorptions.

In this chapter, we provide an overview of common HVIs associated with Canopy Structure (**14.2.1**), Canopy Biochemistry (**14.2.2**) and Canopy Physiology (**14.2.3**). Canopy Biochemistry is further divided into Pigments (**14.2.2.1**), Moisture (**14.2.2.2**) and Plant Residues (**14.2.2.3**). Many of the most commonly used HVIs, with their equations and key citations, are found in Table 14.1. We conclude with two applied examples: one study examining the relationship between LAI and HVIs for *Populus* (**14.3.1),** and another evaluating the relationship between HVIs and seasonal environmental changes for two plant species (**14.3.2**).

Table 14.1 List of the major Hyperspectral Vegetation Indices, including relevant formulas and key citations. Indices marked in grey are ones that serve multiple purposes.

Index	Equation	Reference
Structure (LAI, green biomass, fraction)		
*NDVI	$(R_{NIR}-R_{red})/(R_{NIR}+R_{red})$	Rouse et al.[15]
*SR	R_{NIR}/R_{red}	Jordan [3]
*EVI	$2.5*(R_{NIR}-R_{red})/(R_{NIR}+6*R_{red}-7.5*R_{blue}+1)$	Huete et al.[23]
*NDWI	$(R_{857}-R_{1241})/(R_{857}+R_{1241})$	Gao [29]
**WBI	R_{900}/R_{970}	Peñuelas et al.[28]
*ARVI	$(R_{NIR}-[R_{red}-\gamma*(R_{blue}-R_{red})])/(R_{NIR}+[R_{red}-\gamma*(R_{blue}-R_{red})])$	Kaufman & Tanré [22]
*SAVI	$[(R_{NIR}-R_{red})/(R_{NIR}+R_{red}+L)]*(1+L)$	Huete [21]
**1DL_DGVI	$\sum_{\lambda_{624\,nm}}^{\lambda_{793\,nm}}\|R'(\lambda_i)-R'(\lambda_{626\,nm})\|\Delta\lambda_i$	Elvidge & Chen [1]
**1DZ_DGVI	$\sum_{\lambda_{624\,nm}}^{\lambda_{793\,nm}}\|R'(\lambda_i)\|\Delta\lambda_i$	Elvidge & Chen [1]
*VARI	$(R_{green}-R_{red})/(R_{green}+R_{red}-R_{blue})$	Gitelson et al.[13]
*VIgreen	$(R_{green}-R_{red})/(R_{green}+R_{red})$	Gitelson et al.[13]
Biochemical		
Pigments		
**SIPI	$(R_{800}-R_{445})/(R_{800}-R_{680})$	Peñuelas et al. [31]
**PSSR	(R_{800}/R_{675}); (R_{800}/R_{650})	Blackburn [30]
**PSND	$[(R_{800}-R_{675})/(R_{800}+R_{675})]$; $[(R_{800}-R_{650})/(R_{800}+R_{650})]$	Blackburn [32]
**PSRI	$(R_{680}-R_{500})/R_{750}$	Merzlyak et al. [33]
Chlorophyll		
**CARI	$[(R_{700}-R_{670})-0.2*(R_{700}-R_{550})]$	Kim [34]
**MCARI	$[(R_{700}-R_{670})-0.2*(R_{700}-R_{550})]*(R_{700}/R_{670})$	Daughtry et al. [35]
**CI$_{red\ edge}$	$R_{NIR}/R_{red\ edge}-1$	Gitelson et al. [36]
Anthocyanins		
**ARI	$(1/R_{green})-(1/R_{red\ edge})$	Gitelson et al.[40]
**mARI	$[(1/R_{green})-(1/R_{red\ edge})]*R_{NIR}$	Gitelson et al. [36]
**RGRI	R_{red}/R_{green}	Gamon & Surfus [7]
**ACI	R_{green}/R_{NIR}	Van den Berg & Perkins [41]
Carotenoids		
**CRI1	$(1/R_{510})-(1/R_{550})$	Gitelson et al.[42]
**CRI2	$(1/R_{510})-(1/R_{700})$	Gitelson et al. [42]
Water		
*NDII	$(R_{NIR}-R_{SWIR}/(R_{NIR}+R_{SWIR})$	Hunt & Rock [12]
*NDWI, **WBI	See Above	See Above
*MSI	R_{SWIR}/R_{NIR}	Rock et al. [43]
Lignin &Cellulose/Residues		
**CAI	$100*[0.5*(R2031+R2211)-R2101]$	Daughtry [47]
**NDLI	$[\log(1/R_{1754})-\log(1/R_{1680})]/[\log(1/R_{1754})+\log(1/R_{1680})]$	Serrano et al. [48]
Nitrogen		
**NDNI	$[\log(1/R_{1510})-\log(1/R_{1680})]/[\log(1/R_{1510})+\log(1/R_{1680})]$	Serrano et al. [48]
Physiology		
Light Use Efficiency		
RGRI,SIPI	See Above	See Above
**PRI	$(R_{530}-R_{570})/(R_{530}+R_{570})$	Gamon et al. [9]
Stress		
*MSI	See Above	See Above
**REP	l(max first derivitive: 680-750 nm)	Horler et al. [10]
**RVSI	$[(R_{714}+R_{752})/2-R_{733}$	Merton & Huntington [52]

*Narrow band equivalent of a broad band index
** Strictly narrow-band/hyperspectral

14.2 Applications of Hyperspectral Vegetation Indices (HVIs)

Most structural indices were developed for broad-band systems but have narrow band (<= 10 nm) equivalents (Table 14.1). Exceptions include indices based on first derivatives and the Water Band Index (WBI [28]), which includes wavelengths that are not sampled by broad-band systems (Table 14.1). In contrast, most biochemical/physiological indices are strictly hyperspectral, requiring narrow bands (<= 10 nm) and specific band centers that are not sampled by broad band systems. Band centers and spectral sampling were typically defined by field or laboratory instrumentation used in the original research, but can be modified for alternate systems.

14.2.1 Vegetation Structure (i.e. LAI, FPAR)

Using VIs for vegetation analysis dates back to Jordan [3], who proposed the SR to estimate over-story LAI. Normalized forms of the SR, such as the Normalized Difference Vegetation Index (NDVI: [15]), were proposed soon after and were designed to reduce the impact of atmospheric scattering by using a normalized difference between two bands. Both the SR and NDVI are good predictors of wet and dry green biomass [4], LAI [3], FPAR [5] and fractional cover [16-17]. However, NDVI saturates at high LAI values [14] and varies with viewing geometry [18] and substrate reflectance [19]. Narrow-band versions of the NDVI have been proposed by Galvao et al. [2] and Thenkabail et al. [20], in which wavelength selection was optimized to reduce sensitivity to non-photosynthetic vegetation [2] or to improve crop-specific estimates of LAI, wet biomass and canopy height [20].

Other indices based on NDVI have been proposed to improve canopy structure estimates and minimize the impact of the atmosphere and substrate. For example, the Soil Adjusted Vegetation Index (SAVI:[21]) includes an offset in the denominator designed to force the NDVI to radiate

from the origin of a NIR and red scatterplot, independent of a change in substrate reflectance. The Atmospherically Resistant Vegetation Index (ARVI: [22]) includes a blue band in the numerator and denominator and a weighting factor to compensate for enhanced atmospheric scattering in red wavelengths. The Enhanced Vegetation Index (EVI: [23]) incorporates both a substrate reflectance correction (i.e., SAVI) and a blue band to compensate for the atmosphere (i.e., ARVI). EVI has largely replaced NDVI as a primary global product because of improved resistance to the atmosphere and less evidence of saturation at high LAI [24].

Visible-reflectance variants of the NDVI and ARVI have also been proposed, with the NIR band replaced by a green band, such as the VIGreen and the Vegetation Atmospherically Resistant Index (VARI: [13]). These indices respond more linearly to changes in vegetation cover fraction than does NDVI [13]. VARI has also proven to be highly effective for estimating LAI and moisture stress in maize [25,27] and Live Fuel Moisture (LFM) in shrub lands [26].

Changes in LAI also impact the shape and position of the red-edge and the expression of liquid water in canopy spectra [1,14]. Elvidge and Chen [1] proposed several indices based on the red edge, using first derivative spectra between 626 and 796 nm (1DZ_DGVI and 1DL_DGVI). The relationship between these indices and LAI is significantly improved (compared to other normalized indices) because the slope of the red-edge is more sensitive to changes in LAI and the first derivative spectrum is less sensitive to changes in albedo. Although Elvidge and Chen [1] proposed a range between 626 and 796 nm, hyperspectral systems offer numerous possibilities for alternate, narrower or broader spectral ranges for integration that could be explored. Indices that contrast liquid water absorption, either at 970 or 1200 nm to NIR reflectance outside of these wavelengths such as the Water Band Index (WBI: [28]) and the Normalized Difference Water Index (NDWI: [29]) are also sensitive to LAI. Perry and Roberts

[27] found WBI and NDWI to be the most sensitive of fifteen indices to a change in maize biomass.

14.2.2. Canopy chemistry

14.2.2.1 Plant pigments

A number of indices have been developed to measure overall pigment concentrations or to quantify specific pigments in plant leaves and canopies. Three types of plant pigments contribute significantly to visible reflectance in leaves and canopies: chlorophylls (a and b), carotenoids, and anthocyanin (Figure 14.2). Many indices are formulated either as a simple ratio, such as the Pigment Specific Spectral Ratio (PSSR: [30]) or a normalized ratio, such as the Structurally Insensitive Pigment Index (SIPI: [31]) or the Pigment Sensitive Normalized Difference (PSND: [32]). These indices respond to either a single pigment or combinations, such as the ratio of carotenoids to chlorophyll a (SIPI). Similar to SIPI, the Plant Senescence Reflectance Index (PSRI: [33]) also changes in response to a change in the ratio of carotenoids to chlorophyll as plants senesce.

Indices developed to estimate chlorophyll content include the Chlorophyll Absorption in Reflectance Index (CARI: [34]), Modified CARI (MCARI: [35]) and Chlorophyll Red-Edge Index (CI$_{red\ edge}$: [36]). CARI quantifies the 670 nm chlorophyll absorption feature as the mathematical difference between 700 and 670 nm reflectance, adjusted by a weighted difference between 700 and 550 nm to compensate for non-photosynthesizing materials [38]. MCARI further adjusts the soil compensating component by the ratio of NIR to red reflectance. It has proven effective in identifying nutrient stress in maize [27] and drought stress in Amazonian forests [38]. CI$_{red\ edge}$ is based on a three band generalized model for quantifying pigments [25].

In this model, the concentration of an absorber is quantified as the mathematical difference in reciprocal reflectance, $R_{\lambda 1}^{-1}$, within an absorption region and reciprocal reflectance at a second wavelength, $R_{\lambda 2}^{-1}$, outside of the main absorption region but with similar backscattering. This quantity is multiplied by NIR reflectance to compensate for backscatter dependent variation in brightness. $CI_{red\ edge}$ simplifies to the form shown in Table 14.1 because $R_{\lambda 2}^{-1}$ and R_{NIR} are the same. $CI_{red\ edge}$ has shown a near linear relationship to chlorophyll content over a diversity of broadleaf tree species [39]. In addition to chlorophyll-specific indices, a number of the structural indices have also been used effectively to estimate chlorophyll at leaf scales, such as the SR [37].

Anthocyanins are plant pigments that can increase in response to environmental stress and may play a role in minimizing photoinhibition [40]. Two indices proposed by Gitelson et al. [36, 40] are based on the same concept of reciprocal reflectance developed for chlorophyll, but adjusted for anthocyanin. These include the Anthocynanin Reflectance Index (ARI), calculated as the difference between reciprocal green reflectance (540-560 nm) and reciprocal red-edge reflectance (690-710 nm), and the Modified ARI, which weights ARI by NIR reflectance (760-800 nm). Additional indices built upon the simple ratio model include the red/green ratio (RGRI: [7]) and the Anthocyanin Content Index (ACI: [41]), calculated as the ratio of green to NIR reflectance. RGRI is based on the concept that high anthocyanin content, which results in red leaves, will increase the green to red ratio, while ACI should also increase in response to increased anthocyanins as green leaf reflectance drops.

Carotenoids aid in the process of light harvesting for photosynthesis and protect chlorophyll from photooxidation via the reversible conversion of the xanthophylls violaxanthin to zeaxanthin [9, 42]. They are most readily apparent in leaves during senescence, as they are retained while chlorophyll breaks down. Carotenoid indices include SIPI [31] and two reciprocal reflectance

models proposed by Gitelson et al. [42]; one using the difference between reciprocal reflectance at 510 and 550 nm, the other replacing the 550 nm band with a band at 700 nm (Carotenoid Reflectance Index: CRI1 and 2: 42). The most widely used caretonoid index, however, is the Photochemical Reflectance Index (PRI: [9]), which is designed to capture the shift from violaxanthin to zeaxanthin. This transition results in a subtle (< 1%) decrease in reflectance at 531 nm that can be quantified using a normalized difference index and 570 nm as the reference band [9]. In this form, increasingly negative PRIs will occur with increasing plant stress. The PRI is discussed in more detail in Section 14.2.3.

14.2.2.2 Canopy moisture
Plant canopy moisture varies as a function of the number of leaves within a crown (Figure 14.1) and the water content of individual leaves (Figure 14.2). Simple ratio and normalized indices have been proposed to compare the expression of subtle or strong liquid water bands relative to a reference non-absorbing wavelength. Simple ratios include the Moisture Stress Index (MSI: [43]) and the WBI [28]. The MSI is calculated as the ratio of a SWIR band (1650 nm) to NIR band (830 nm), while the WBI is calculated as the reflectance ratio of 900 nm to 970 nm. Increases in water content correspond with decreases in the MSI and increases in the WBI. Normalized versions of the MSI include the Normalized Difference Infrared Index (NDII: [12]), in which the SWIR band can either be at a short wavelength (1650 nm) or long-wavelength (2200 nm). The NDWI [29] is roughly equivalent to the normalized version of the WBI, although the 1240 nm water band takes the place of the 970 nm band.

Several studies have evaluated the relationship between moisture indices and relative water content (RWC: [44]), plant water content [29], LFM [26] and moisture stress [12,27,43]. Serrano et al. [44] found WBI and NDWI performed better than NDVI and NDII in shrublands, and

Penuelas et al. [29] found a strong correlation between the WBI and plant water content across a wide range of Mediterranean ecosystems. Roberts et al. [26] found WBI and NDWI superior to NDVI, EVI and NDII for estimating LFM. Several forms of the WBI, including water absorption features at 960, 1180 and 1450 nm were tested to determine their ability to estimate water content for leaves, thin tissues (i.e. stems) and leaves and thin tissues [45]. The 960 and 1180 nm WBI were the most strongly correlated with thin tissue water ($r^2 > 0.75$) over a wide range of plant functional types with slightly higher correlations found for 1180 nm.   It should be noted that two greenness measures, the VIG and VARI, have consistently shown stronger relationships to moisture stress than other greenness or water based indices [27,26], potentially because water stress also manifests as an increase in green reflectance [46].

14.2.2.3 Lignin and Cellulose/Plant Residues

Specific absorption bands associated with proteins, starch, sugars, lignin and cellulose, make HVIs especially well-suited for measuring the biochemistry of branches or senesced plant materials in the absence of water and pigments ([6]; Figure 14.2). Of these biochemicals, two of the most evident in reflectance spectra are lignin and cellulose, which produce many prominent absorption features in the SWIR. Several HVIs have been developed specifically to estimate the ligno-cellulose content or mass of senesced plant materials, including the Cellulose Absorption Index (CAI: [47]) and the Normalized Difference Lignin Index (NDLI: [48]). The CAI is a band-depth measure, calculated as the difference in reflectance within a strong cellulose absorption band at 2101 nm and average reflectance for two bands outside of this absorption feature, at 2031 and 2211 nm. The NDLI targets a prominent lignin absorption band at 1754 nm and uses a normalized difference index formula but with the natural logarithm of reciprocal

reflectance, a common transform used in biochemical spectroscopy (e.g., [49]). Serrano et al. [48] also proposed a similar index targeted at the 1510 nm N absorption feature, called the Normalized Difference Nitrogen Index (NDNI). Both normalized indices use the non-absorbing 1680 nm band as a reference band.

Daughtry et al. [17] evaluated the performance of CAI and NDVI for estimating fractional cover of crop residues and green cover for corn, soybean and wheat over several soils for cases of dry and wet residual biomass. They noted that the CAI and NDVI were essentially uncorrelated, with CAI strongly linearly correlated to changes in the fraction of crop residues and NDVI strongly correlated to changes in green cover for all crops and conditions. When applied to AVIRIS data the combination of CAI and NDVI enabled them to accurately discriminate conservation, reduced and intensively tilled soils [50], which is critical in assessing soils for potential erosion or carbon uptake. Serrano et al. [48] analyzed AVIRIS data acquired from drought deciduous and evergreen chaparral species, finding a strong linear relationship between NDLI and NDNI for bulk lignin and nitrogen, respectively.

14.2.3. Plant Physiology

Leaf physiology also impacts reflectance spectra. A good example is how the position and shape of the red-edge shifts in response to plant stress, either towards shorter wavelengths (blue shift) or longer wavelengths (red shift: [10]). Blue shifts were reported by Rock et al. [43] and Horler et al. [10], in response to heavy metal stress in *Picea* [43] and *Pisum* [10]. Red-shifts typically occur during chlorophyll development, and nutrient stress sometimes decreases this shift [51]. A quantitative measure of the position of the red-edge is the maximum of the first derivative of reflectance between 650 and 750 nm [10]. Merton and Huntington [52] proposed the Red-edge Vegetation Stress Index (RVSI), an index that captures variation in shape of the

red-edge associated with plant stress. The RVSI is calculated as the average canopy reflectance at 714 and 752 nm, minus reflectance at 733 nm. A concave upward red edge and slightly negative or positive RVSI is found in stressed plants, while a concave downward red-edge, and strongly negative RVSI occurs in unstressed plants [52]. Naidu et al. [53], studying leafroll-infected grape vines, found stressed leaves had slightly less negative RVSI values than healthy leaves. In contrast, Perry and Roberts [27] found RVSI to become less negative with higher leaf nitrogen.

The PRI has proven to be one of the most effective stress/physiology-oriented HVIs. As plants become progressively more stressed and are unable to utilize light absorbed by chlorophyll, reflectance at 531 nm drops as violazanthin shifts to zeaxanthin, producing an increasingly negative PRI. As a result, the PRI provides a viable surrogate for measuring Light Use Efficiency (LUE). Gamon et al. [54] evaluated carbon uptake by dry tropical forest species using canopy reflectance. They found NDVI and SR responded primarily to changes in FPAR, while PRI responded to photosynthetic down regulation, becoming increasingly negative at midday. Rahman et al. [55] combined strengths of the NDVI for FPAR and PRI for LUE to develop a multiplicative model for estimating carbon uptake by boreal forests. This model showed a near-linear relationship between NDVI*PRI-predicted carbon uptake, and CO_2 flux measured by several flux towers [55].

14.3 Applications

14.3.1 Estimating LAI using Hyperspectral Vegetation Indices

We evaluate several structurally-oriented HVIs for estimating LAI of hybrid poplars (*Populus trichocarpa*). The original study, described in Roberts et al. [56], was designed to

evaluate the relationship between LAI and the expression of liquid water in canopies. Here we focus strictly on HVIs, adding several that were not evaluated in the original study.

The study site is located near Wallula, Washington (46° 4' N, 118° 54' W), at the Boise-Cascade Wallula fiber farm. Field work was conducted between 20 and 25 of July 1997. Seventy-six young stump-sprouting plants, ranging between 10 and 60 cm in height were sampled in a six-year old stand that had been recently harvested. Reflectance spectra were measured above each plant using an Analytical Spectral Devices (ASD) full range instrument (Analytical Spectral Devices, Boulder, CO) and standardized to reflectance with a spectralon panel (Labsphere Inc. North Sutton, NH) measured at approximately 10 minute intervals. At least three replicates were measured for each plant. One to four sets of spectra were measured per plant depending on the size of the re-sprout at a height of 0.5 m above the canopies. In order to determine LAI, plants were destructively harvested, with five plants randomly sampled in each of five height classes designed to ensure a range in LAI. Plant height and diameter along the major and minor axes were measured to determine ground area cover and plant volume for each plant. Leaf area was calculated for each plant using a linear equation relating stem diameter to leaf area. Stem diameter was measured for every stem on the sampled plants using calipers. In order to develop the linear equation relating leaf area to stem diameter, one out of every ten stems was stored in a plastic bag, cooled, and then transported to the laboratory for analysis. Leaves from each stem were harvested, measured for leaf area, than regressed against stem diameter. This relationship was then combined with the re-sprout stem data to calculate total leaf area for each re-sprout, and LAI was calculated as leaf area divided by the areal projection of each re-sprout. The analysis included three soil spectra and twenty-four plant spectra. For more details see [56].

LAI increases led to dramatic changes in canopy reflectance, including decreasing visible light reflectance, increasing NIR reflectance, and the increased expression of weak and strong absorption features (Figure 14.1). Eight indices were calculated: two that respond to canopy water (WBI, NDWI), five to greenness (SR, NDVI, EVI, VIG, VARI) and one to the red edge (1DZ_DGVI). All the indices were highly correlated with LAI (Table 14.2, Figure 14.3), and all but NDVI showed a linear relationship, producing r^2 values between 0.69 (WBI) to 0.78 (VARI: Figure 14.3). The NDVI-LAI scatter plot (Figure 14.3 b) illustrates NDVI saturating at high LAI, beginning around an LAI of 4. The water-based indices had the lowest r^2 values, the NIR to red combinations (SR, NDVI and EVI) intermediate, and VIG and VARI were the highest. The red-edge based index (1DZ_DGVI) outperformed the SR and linear NDVI model, but had a slightly lower r^2 than a non-linear fit for NDVI or the linear relationship for the EVI.

Table 14.2 Linear and non-linear relationship between LAI and 8 HVIs. Fit metrics include r^2, Root Mean Squared Error (RMS), Mean Absolute Error (MAE) and variants on the MAE to quantify LAI prediction errors at high LAI (MaxAE) and over bare soils (Soil Error). Only the NDVI-LAI relationship was improved by a non-linear model.

| Fit Metric	WBI	NDWI	SR	NDVI	NDVI(P)	EVI	VIG	VARI	1DZDG
Slope	44.51	34.31	0.38	7.23	8.12	7.28	11.32	8.11	10.15
Intercept	-43.19	1.67	0.27	-1.11	0	-0.75	1.18	1.24	-0.03
Exponent					2.87				
r^2	0.69	0.73	0.74	0.72	0.77	0.77	0.78	0.78	0.76
RMS	0.21	0.2	0.19	0.2	0.18	0.18	0.18	0.18	0.19
MAE	0.9	0.82	0.8	0.77	0.67	0.69	0.65	0.64	0.71
MaxAE	2.29	2.57	2.17	3.47	3.03	3.57	3.13	3.24	3.65
MinAE	0.09	0.01	0.03	0.07	0	0.05	0.03	0.02	0.06
Soil Error	0.23	0.18	0.72	0.42	0	0.25	0.07	0.14	0.21
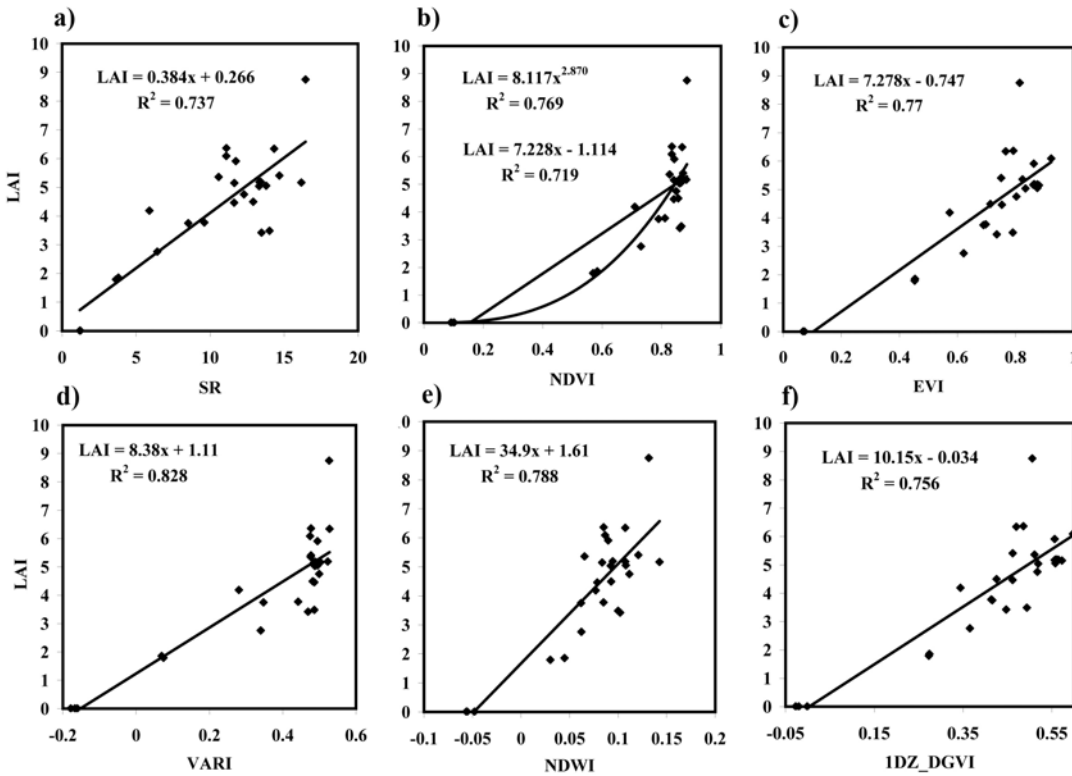
Figure 14.3 Showing scatter plots between LAI (y) and a subset of indices including a) the SR; b) NDVI; c) EVI; d) VARI; e) NDWI and ; f) 1DZ_DGVI.

Error metrics were calculated to examine model differences. The maximum Absolute Error (MaxAE) captures a model's over or under-prediction across the range of LAI values. Based on this error metric, the WBI, NDWI and SR all produced considerably lower errors than the greenness measures, demonstrating that though the greenness measures fit the total population better, they under-predicted high LAI values, suggesting water-based indices and the SR are likely to perform better in high LAI forests. Soil Error was calculated as the average mean absolute error for predictions of LAI over bare soils. A high value indicates that an index will produce an error in LAI when cover is sparse or absent. Based on this metric, the lowest error occurred for a power function fit of the NDVI, followed closely by VIG and VARI. The highest Soil Error observed was for the SR, equal to nearly one LAI, suggesting that the SR is not effective for sparsely covered areas. The second highest error was for the NDVI linear model,

equal to 0.5 LAI. EVI had a lower Soil Error than NDVI as would be expected given the formulation of EVI.

14.3.2 Soil Moisture and AET

In the second example, we focus on how seasonal changes in soil moisture impact the reflectance spectra and HVI values for two invasive species. We extend the analysis to evaluate the relationship between several HVIs and measures of potential (PET) and actual (AET) evapotranspiration, calculated using Penman Monteith [57] and the Bowen Ratio[58], respectively. This study was conducted at Coal Oil Point Reserve (COPR), California, one of three areas sampled by the Innovative Datasets for Environmental Analysis by Students (IDEAS) network (www.geog.ucsb.edu/ideas: [59]). Additional data shown include webcam imagery used to track changes in canopy greenness at solar noon for annual and perennial plants [60].

COPR is located at 34.41386° N and119.8802° W at an elevation of 6 m and is dominated by a mixture of native and invasive annual grasses and forbs and perennial shrubs. The micrometeorological tower at COPR measures all variables needed to calculate PET and AET, including wind speed and direction, air temperature and relative humidity (at 0.75 and 2.85 m) and net radiation using a four-channel net radiometer. Additional instrumentation includes a tipping bucket rain gauge, fog collector and leaf wetness sensor. Three below-ground sensors measure soil temperature and volumetric water content at 10, 20 and 50 cm. Soil heat flux, G, was estimated from a combination of soil temperature at 10 cm and surface temperature using an assumed thermal conductivity of 0.4 $Wm^{-1}K^{-1}$. Soils at COPR are clay-loams with clay content increasing from 29.6 to 35.7% from 10 to 50 cm. For more details on instrumentation or site properties see www.geog.ucsb.edu/ideas.

Seasonal environmental data, plotted over two years starting in November, 2007, illustrate a typical Mediterranean climate, defined by winter precipitation and summer drought (Figure 14.4a). Rainfall was highly variable between years, with almost all of the rainfall in the 2007-2008 hydrological year falling in a single month. In 2008-2009, the rains started earlier and persisted longer, but totaled less. Soil moisture responded rapidly to precipitation, with the greatest seasonal fluctuations at the shallowest depths and a rapid increase followed by a more gradual dry down (Figure 14.4c). Overall, soil moisture remained relatively high due to the high clay content of soils in the study region.
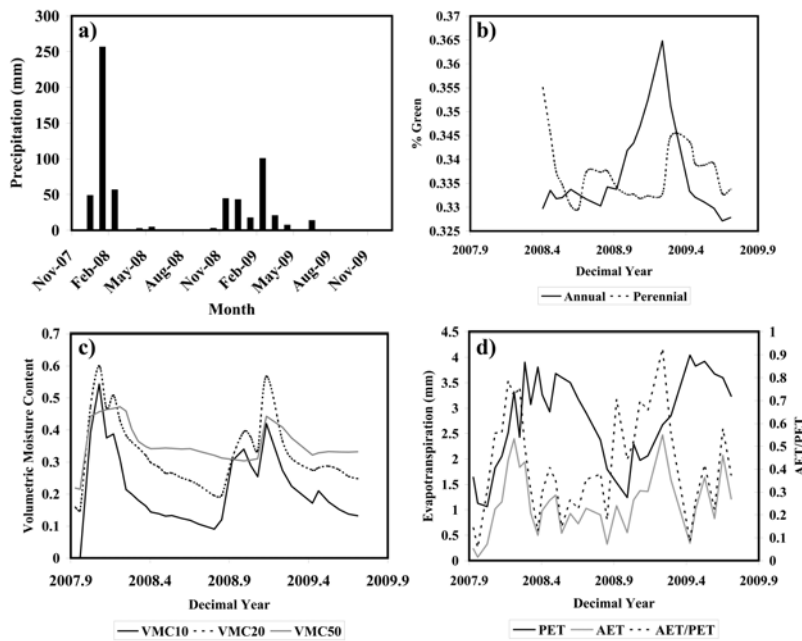
Figure 14.4 Showing (a) precipitation; (b) webcam % green; (c)Volumetric Soil Moisture (VMC) at 10, 20 and 50 cm and d) PET, AET and AET/PET.

A webcam, deployed in the late spring of 2008 shows the pronounced, but distinct seasonal cycle of annual and perennial vegetation (Figure 14.4b). Solar noon images were analyzed using software described in [60] to generate estimates of percent greenness for uniform regions of annuals and perennials. PET, AET and the ratio of AET to PET also show pronounced seasonal cycles as would be expected (Figure14.4d). PET, to a large extent, is driven by a combination of

net radiation and vapor pressure deficit (VPD), and thus peaks in the summer when the skies are clear and the air is dry. AET, by contrast, is controlled by available moisture, as well as net radiation and VPD and thus peaks in the spring, when soil water is plentiful and can either be directly evaporated from the surface, or transpired by green plants. Based on the ratio of AET to PET, between 80 and 90% of the atmospheric moisture demand was met by ET in the spring, yet typically less than 20% over the summer.

Reflectance spectra were collected of two invasive plants species in the area over two hydrological years starting in October, 2007. Species measured included *Brachypodium distachyon* (BRDI: Purple false brome) and *Carduus pycnocephalus* (CAPY: Italian thistle). Spectra were collected over five individuals of each species by measuring 25 spectra for each individual plant, five at the plant center and in the four cardinal directions from approximately 0.5-1 m above the canopy. Spectra were acquired within 2 hrs of solar noon at two to four week intervals using an ASD spectrometer and a spectralon standard.

Bi-weekly reflectance spectra demonstrate significant variation in plant responses to changes in moisture, temperature and net radiation (Figure 14.5). BRDI started the year highly senesced, beginning to green up by Julian day (JD)77 (Figure 14.5a). Peak greenness was reached quickly by JD137 followed by a rapid senescence. While chlorophyll and water absorption features are evident, they were never expressed as clearly as might be expected for an individual leaf. Furthermore, ligno-cellulose absorptions were evident through out the year, becoming the dominant absorption feature by JD167. After senescence, BRDI spectra continued to evolve, showing a gradual decrease in reflectance and change in convexity of the visible-NIR region as stems became decomposed.

Unlike BRDI, CAPY showed very pronounced chlorophyll and liquid water absorptions and had a well-defined, steeply sloping red-edge (Figure 14.5b). Furthermore, CAPY greened up earlier than BRDI and remained active far longer into the growing season. For example, on JD167, when BRDI was fully senesced, CAPY still showed a pronounced red-edge and chlorophyll absorptions, although ligno-cellulose bands also suggest it was senescing. By JD197 CAPY was senesced, but had lower reflectance than BDRI because of its taller canopy.

A subset of HVIs were calculated from reflectance spectra to explore the relationship between HVIs and soil moisture and ET (Figure 14.6). In this Figure, BRDI is shown on the left and CAPY on the right. Temporal plots for three indices, $CI_{red\ edge}$ (chlorophyll), WBI (Water) and RVSI (Stress) are plotted with VMC20 and the ratio of AET to PET. All indices show a clear seasonal pattern that corresponds well to soil moisture, illustrating the strong dependence of plant growth on soil moisture in a Mediterranean climate. However, VMC20 and the HVIs are not perfectly aligned. For example, in 2008 the WBI significantly lags the peak in soil moisture, while $CI_{red\ edge}$ lacks VMC20 asymmetry. RVSI, interestingly, appears to capture some of the asymmetry in soil
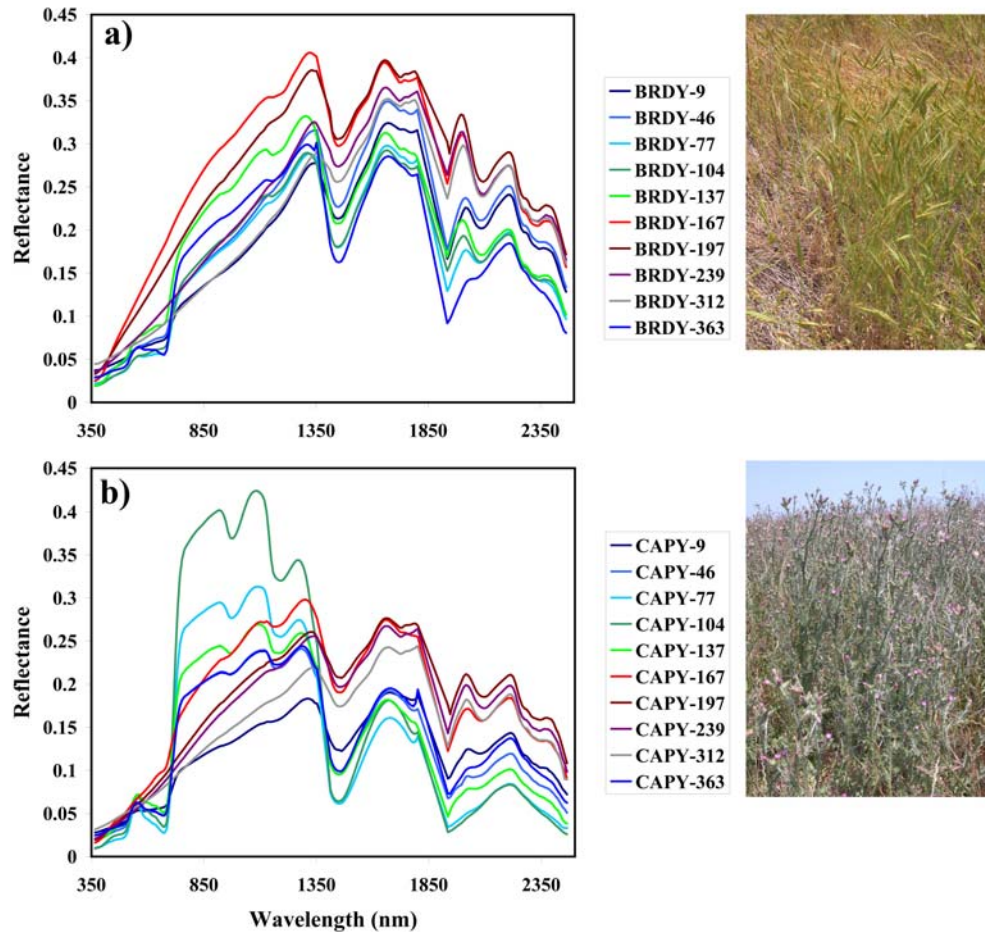
Figure 14.5 Reflectance spectra of *Brachypodium distachyon* (BRDI) and *Carduus pychnocephalus* (CAPY) for 2009. The number to the right on the legend reports Julian day.

moisture in 2008. In 2009, all three indices were better aligned with VMC20. Furthermore, indices calculated for CAPY tend to better track seasonal changes in VMC20, particularly in 2008.

The HVIs align far better with the ratio of AET to PET than with VMC20. The peak in $CI_{red\ edge}$ and WBI, and trough in RVSI align very well with peak AET/PET for CAPY. For BRDI, $CI_{red\ edge}$ and RVSI match AET/PET, but WBI is clearly lagged in 2008, in which peak AET occurs well before peak WBI. Better alignment for CAPY, suggests that AET at the site may be largely controlled by the seasonal response in this species, which was already photosynthetically

active by January and thus was able to take advantage of early winter rains and remain green as

long as enough moisture was available to support high AET. Better alignment for AET than

VMC20 is not surprising, given that VMC can be high when plants are completely senesced, yet

AET will only be high when plants are green if transpiration is a major contributor to ET.
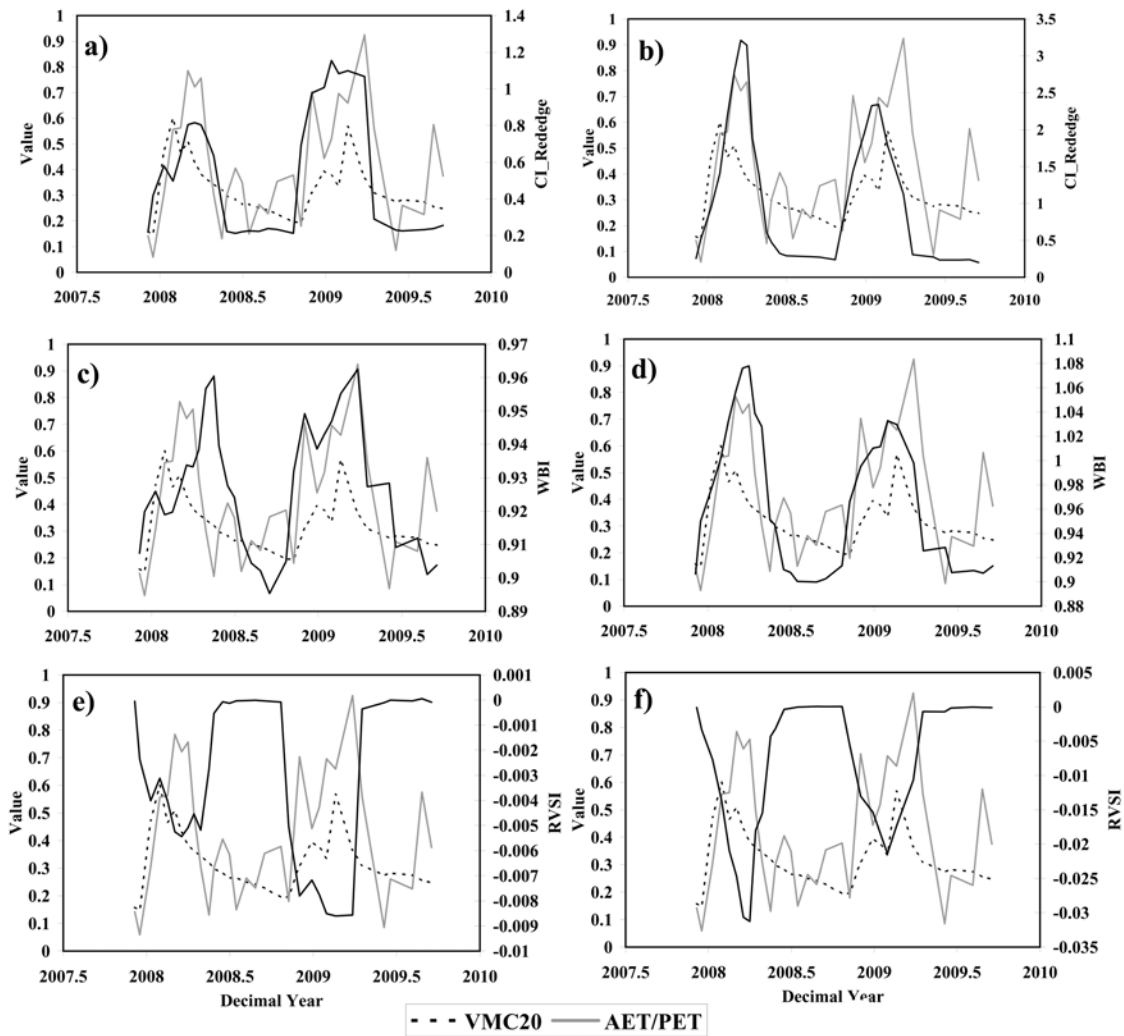
Figure 14.6 Time series plots of VMC20 (dashed), AET/PET (solid) and HVI values for
BRDY (a,c,e) and CAPY (b,d,f) for CI-rededge (a,b), WBI (c,d) and RVSI (e,f).

Statistical relationships between HVIs and environmental measures were evaluated by

regressing a selection of HVIs against each of the measures over a two year period for each

species (Figure 14.7: Tables 14.3 and 14.4). Many HVIs proved to show statistically significant

relationships to VMC at 10 or 20 cm depth, PET, or AET/PET. For example, CRI1, had the

highest r^2 value with soil moisture, followed closely by NDVI for BRDI (Table 14.3).
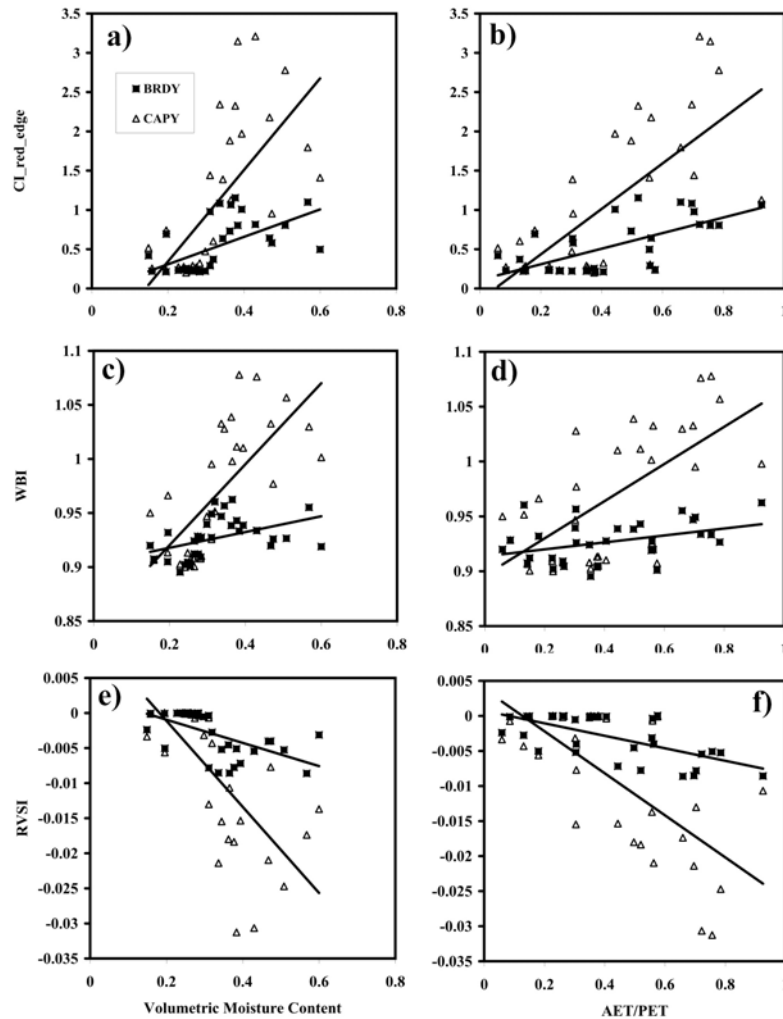
Figure 14.7 scatterplots between VMC (a, c, e) and AET/PET (b, d, f) for three HVIs, CI_rededge, WBI and RVSI for BRDY (solid squares) and CAPY (open triangles).

For this shallow-rooted species, higher correlations were observed for 10 cm than 20 cm. Other

indices that showed a strong correlation with soil moisture included all of the pigment and

greenness measures, the NDNI, NDLI and RVSI. The water based indices showed a poorer

relationship and no significant relationship was observed for PRI.   Most indices were positively

correlated to VMC and AET, although RVSI was negatively correlated, consistent with

increasingly positive RVSI with increasing plant stress [52].

Table 14.3 Statistical relationships using linear regression for BRDI for 21 HVSIs. Statistical significance is reported as (* = 0.05, **=0.01, *** =0.001)

	VMC10	VMC20	PET	AET	AET/PET		VMC10	VMC20	PET	AET	AET/PET
Greenness			r^2						F-Stat		
DL1DGVI	0.302	0.295	0.043	**0.136**	0.342		13**	12.5**	1.3	4.7*	15.6***
DZ1DGVI	0.363	0.31	0.268	0.096	0.402		17.1***	13.9***	11**	3.1	20.2***
EVI	0.372	0.334	0.101	0.123	0.411		17.8***	15***	5.8*	4.2*	21***
NDVI	**0.414**	**0.367**	0.257	0.123	0.444		21.2***	17.4***	10.4**	4.2*	23.9***
SR	0.37	0.312	0.242	0.121	**0.448**		17.6***	13.6***	9.6**	4.2	24.4***
VARI	0.295	0.208	**0.51**	0.01	0.239		12.6**	7.9**	32***	0.3	9.4**
Pigments											
ARI2	0.308	0.321	0.018	**0.259**	0.454		13.3***	14.2***	0.6	10.5**	24.9***
CI_rededge	0.377	0.335	0.242	0.139	0.463		18.2***	15.1***	9.6**	4.9*	25.8***
CRI1	**0.429**	**0.397**	0.209	0.157	**0.477**		22.6***	19.8***	7.9**	5.6*	27.4***
MCARI	0.352	0.284	0.251	0.065	0.357		10.3***	11.9**	10**	2.1	10.7***
SIPI	0.332	0.291	**0.404**	0.055	0.311		14.9***	12.3**	20.4***	1.7	13.6***
Nitrogen											
NDNI	0.391	0.318	0.571	0.003	0.221		19.2***	14***	40***	0.1	8.5**
Water											
MSI	**0.173**	**0.194**	0.004	**0.147**	0.221		6.3*	7.2*	0.1	5.2*	8.5**
NDII	0.136	0.154	0.004	0.146	**0.222**		4.7*	5.5*	0.1	5.1*	8.6**
NDWI	0.073	0.086	0.014	0.076	0.116		2.4	2.8	0.4	2.5	3.9
WBI	0.155	0.185	**0.027**	0.048	0.15		5.5*	6.8*	0.8	1.5	5.3*
Cellulose/Residues											
CAI	0.299	0.195	**0.558**	0.007	0.249		12.8**	7.2*	37.9***	0.2	9.9**
NDLI	**0.328**	**0.343**	0.02	**0.178**	**0.347**		14.6***	15.6***	0.6	6.5*	15.9***
Plant Stress/Physiology											
PRI	0.054	0.096	0.206	**0.12**	0.056		1.7	3.2	7.8**	4.1	1.8
RVSI	**0.371**	**0.332**	**0.259**	0.104	**0.413**		17.7***	14.9***	10.5**	3.5	21.1***

.

Several indices were strongly correlated to PET, most likely driven by a strong relationship

to net radiation. These included VARI, SIPI, NDNI and CAI. The poorest relationships were

observed for AET. By contrast, the highest r^2 values were observed for AET/PET, with most

greenness measures producing r^2 values greater than 0.4, and CRI1 producing the highest r^2

value of 0.477, followed closely by $CI_{red\ edge}$ and ARI2.

Table 14.4 Statistical relationships using linear regression for CAPY for 21 HVSIs. Statistical significance is reported as (* = 0.05, **=0.01, *** =0.001)

	VMC10	VMC20	PET	AET	AET/PET		VMC10	VMC20	PET	AET	AET/PET
Greenness			r^2						F-Stat		
DL1DGVI	0.348	0.452	0.027	**0.336**	**0.506**		15.5***	23.9***	0.8	14.7***	29.7***
DZ1DGVI	0.369	0.448	0.084	0.259	0.48		16.9***	23.6***	2.7	10.2**	26.7***
EVI	0.388	0.476	0.057	0.289	0.501		18.4***	26.3***	1.8	11.8**	29.1***
NDVI	**0.48**	**0.534**	0.143	0.191	0.464		26.8***	33.2***	4.9*	6.8*	25.1***
SR	0.326	0.401	0.054	0.291	0.476		14***	19.4***	1.7	11.9**	26.4***
VARI	0.432	0.452	**0.213**	0.13	0.389		22***	23.9***	7.9**	4.3*	18.5***
Pigments											
ARI2	0.208	0.329	0.007	**0.433**	0.472		7.6**	14.2***	0.2	22.1***	25.9***
CI_rededge	0.387	**0.451**	0.091	0.246	**0.476**		18.3***	23.8***	2.9	9.5**	26.3***
CRI1	**0.542**	0.439	**0.803**	0.038	0.37		9.5*	6.3*	32.6***	0.3	4.7
MCARI	0.327	0.423	0.043	0.323	0.5		14.1***	21.3***	1.3	13.8***	29***
SIPI	0.397	0.423	0.3	0.059	0.293		19.1***	21.2***	12.4**	1.8	12**
Nitrogen											
NDNI	0.491	0.507	0.143	0.196	0.482		28***	29.8***	4.8*	7.1*	27***
Water											
MSI	**0.443**	**0.517**	**0.109**	0.163	0.396		23.1***	31.1***	3.6	5.7*	19***
NDII	0.404	0.504	0.064	**0.253**	**0.464**		19.7***	29.5***	2	9.8**	25.1***
NDWI	0.421	0.508	0.081	0.228	0.451		21.1***	29.9***	2.5	8.6**	23.8***
WBI	0.42	0.501	0.109	0.212	0.438		21***	29.1***	3.5	7.8**	22.6***
Cellulose/Residues											
CAI	0.335	0.393	**0.21**	0.125	0.376		14.6***	18.7***	7.7**	4.1	17.4***
NDLI	**0.41**	**0.517**	0.044	**0.261**	**0.457**		20.2***	31.1***	1.3	10.2**	24.4***
Plant Stress/Physiology											
PRI	0.11	0.056	**0.598**	0.036	0.026		3.6	1.7	43.1***	1.1	0.8
RVSI	**0.391**	**0.47**	0.083	**0.256**	**0.48**		18.6***	25.7***	2.6	10**	26.8***

Similar correlations were observed for CAPY, although r^2 values tended to be considerably higher, as might be expected based on the better temporal match between VMC, AET and reflectance changes in CAPY. The highest r^2 value for this species was 0.803, between the CRI1 and PET. This pigment index differed starkly from all other pigment indices, which showed typically poor relationships with PET. Very high r^2 values were also observed between greenness measures and VMC, with VMC at 20 cm showing a slightly stronger relationship (in contrast to BRDI). Pigment measures were similarly highly correlated with VMC, although the highest correlation, with an r^2 value of 0.542 was observed for CRI1 with VMC10. Contrary to BRDI,

HVIs for CAPY were also highly correlated with AET and water-based indices were significantly correlated with soil moisture. Finally, r^2 values between HVIs and AET/PET tended to be higher for CAPY than BRDI.

Overall, we conclude that (1) HVIs are better predictors of AET/PET than soil moisture, (2) these relationships vary significantly between plant species with different phenologies, and (3) while pigment-based and greenness-based indices were effective across species, the performance of water-based indices was more species-dependent. These results show that HVIs can be of great use in applications ranging from individual species identification to quantifying environmental variables where field data is sparse or absent.

14.4 Discussion

Most hyperspectral systems collect a large volume of data in wavelengths that are highly correlated. HVIs are one means by which the wealth of information captured in a spectrum can be distilled to a few, physically meaningful variables. In one form, HVIs take advantage of finer spectral sampling to generate a narrow-band equivalent of a broad band VI. While narrow-band equivalents of broad-band indices have not necessarily improved performance (e.g. [1]), a change in the wavelength position of one or more bands within the index, better tuned for a specific absorption has been shown to significantly improve performance [2,20].

A potentially greater contribution of hyperspectral systems is their ability to create new indices that incorporate wavelengths not sampled by any broad-band system and to quantify absorptions that are specific to an important biochemical and\or biophysical quantities of vegetation. Examples include most of the pigment-oriented indices, all indices formulated for the red-edge, several water absorption indices and indices that use three or more wavelengths in the SWIR. In many cases, these indices have either proven to be less sensitive to saturation, such as

water-based indices for LAI, or less sensitive to changes in lighting/viewing geometry such as VARI [26]. NIR and SWIR based indices, because they sample spectral regions with reduced atmospheric scattering, would be expected to be less sensitive to atmospheric contamination. Some of the most promising HVIs are designed to quantify key plant physiological responses such as the PRI used as a proxy for LUE and RVSI, which is highly sensitive to seasonal changes in environmental stress. There is also considerable potential in combining several indices through multivariate regression to improve a biophysical or biochemical retrieval or as inputs into classification [61]. Such an approach takes advantage of the greater diversity of spectral features available through hyperspectral sensors to improve a retrieval based on multiple measures of the same variable and offers the potential of classifying vegetation based on inferred biochemistry and structure as in [61].

In this chapter, we provided a review of many of the most commonly used and best-adopted HVIs reported in the literature. We strongly linked the formulation of the HVI to its physical basis, typically including at least one strong absorption band and a non-absorbing reference band. To illustrate some of the potential of these indices, we supplied two example case studies. As the number and amount of hyperspectral sensors and data increases, HVIs will become ever more important and prevalent.

REFERENCES

1. Elvidge, C.D., and Chen, Z., Comparison of Broad-band and Narrow-band Red and Near-Infrared Vegetation Indices, *Remote Sensing of Environment*, 54:38-48, 1995.

2. Galvao, L.S., Viterello, I. and Almeida Filho, R.,Effects of Band Positioning and Bandwidth on NDVI Measurements of Tropical Savannas, *Remote Sensing of Environment*, 67: 181-193, 1999.

3. Jordan, C.F., Leaf-Area Index from Quality of Light on the Forest Floor, *Ecology*, 50(4): 663-666, 1969.

4. Tucker, C. J., Red and photographic infrared linear combinations for monitoring vegetation, *Remote Sensing of Environment.* 8:127-150, 1979.

5. Sellers, P. J., Canopy reflectance, photosynthesis and transpiration, *International Journal of Remote Sensing.* 6:1335-1372, 1985.

6. Curran, P.J., Remote Sensing of Foliar Chemistry, *Remote Sensing of Environment*, 30: 271-278, 1989.

7. Gamon J.A., Surfus J.S., Assessing leaf pigment content and activity with a reflectometer. *New Phytologist* 143:105-117, 1999.

8. Ustin, S. L., Gitelson, A.A., Jacquemoud S., Schaepman, M., Asner, G. P., Gamon J. A., and P. Zarco-Tejada. Retrieval of foliar information about plant pigment systems from high resolution spectroscopy. *Remote Sensing of Environment,* 113: S67–S77, 2009.

9. Gamon J,A., Serrano L, Surfus J.S., The photochemical reflectance index: an optical indicator of photosynthetic radiation-use efficiency across species, functional types, and nutrient levels. *Oecologia* 112:492-501, 1997

10. Horler, D. N. H., Dockray, M., and Barber, J., The red-edge of plant leaf reflectance, *International Journal of Remote Sensing.* 4:273-288. 1983.

11. Zarco-Tejada, P.J., Miller, J.R., Mohammed, G.H., and Noland, T.L., Chlorophyll Fluorescence Effects on Vegetation: Apparent Reflectance: Leaf-Level Measurements and Model Simulation, *Remote Sensing of Environment*, 74: 582-595, 2000.

12. Hunt, E. R., Jr. and Rock, B. N., Detection of changes in leaf water content using near- and middle-infrared reflectances, *Remote Sensing of Environment* 30:43-54, 1989.

13. Gitelson A.A., Kaufman Y.J., Stark R., and Rundquist D.' <u>Novel algorithms for remote estimation of vegetation fraction</u>, *Remote Sensing of Environment*, 80: 76-87, 2002.

14. Roberts, D.A., Ustin, S.L., Ogunjemiyo, S., Greenberg, J., Dobrowski,S.Z., Chen, J. and Hinckley, T.M., Spectral and structural measures of Northwest forest vegetation at leaf to landscape scales, *Ecosystems*, 7:545-562, 2004.

15. Rouse, J. W., Haas, R. H., Schell, J. A., and Deering, D. W., Monitoring vegetation systems in the great plains with ERTS, in *Third ERTS Symposium,* NASA SP-351, NASA, Washington, DC, Vol. 1, p. 309-317. 1973.

16. Carlson, T.N., and Ripley, D.A., On the Relation between NDVI, Fractional Vegetation Cover and Leaf Area Index, *Remote Sensing of Environment*, 62: 241-252, 1997.

17. Daughtry, C. S. T., Hunt Jr., E. R., and McMurtrey III, J. E. Assessing crop residue cover using shortwave infrared reflectance. Remote Sensing of Environment 90:126-134. 2004.

18. Deering, D.W., Middleton, E.M., and Eck, T.F. Reflectance anisotropy for a Spruce-Hemlock forest canopy, *Remote Sensing of Environment* , 47:242-260, 1994.

19. Huete, A. R., Jackson, R. D., and Post, D. F. Spectral response of a plant canopy with different soft backgrounds, *Remote Sensing of Environment.* 17:37-53, 1984.

20. Thenkabail P.S., Smith, R.B., and De-Pauw, E. 2000. Hyperspectral vegetation indices for determining agricultural crop characteristics. *Remote sensing of Environment.* 71:158-182. 2000.

21. Huete, A. R., A soil adjusted vegetation index (SAVI), *Remote Sensing of Environment,* 25:295-309, 1988.

22. Kaufman, Y.J., and Tanier, D., Atmospherically Resistant Vegetation Index (ARVI) for EOS-MODIS, *IEEE Transactions on Geoscience and Remote Sensing*, 30(2): 261-270., 1992.

23. Huete, A.R., Liu, H.Q., Batchily, K. and van Leeuwen, W., A Comparison of Vegetation Indices over a Global Set of TM Images for EOS-MODIS, *Remote Sensing of Environment,* 59:440-451,1997.

24. Huete, A.R., Didan, K., Miura, T., Rodriguez, E.P., Gao, X., and Ferreira, L., Overview of the radiometric and biophysical performance of the MODIS vegetation indices, *Remote Sensing of Environment*, 83, 195-213, 2002.

25. Gitelson, A. A., Viña, A., Arkebauer, T. J. ,Rundquist, D. C., Keydan, G., and Leavitt, B., Remote estimation of leaf area index and green leaf biomass in maize canopies, *Geophysical Research Letters*, 30(5), 1248, doi:10.1029/2002GL016450, 2003.

26. Roberts, D.A, Dennison, Peterson, S., P.E., Sweeney, S. and Rechel, J., Evaluation of AVIRIS and MODIS Measures of Live Fuel Moisture and Fuel Condition in a Shrubland Ecosystem in Southern California*, Journal of Geophysical Research Biogeosciences ,* Vol. 111. G04S02, doi: 10.1029/2005JG000113, 16 pp, 2006.

27. Perry, E.M., and Roberts, D.A., Sensitivity of Narrow-Band and Broad-Band Indices for Assessing Nitrogen Availability and Water Stress in Annual Crop, *Agronomy Journal*. Vol. 100(4): 1211-1219, 2008.

28. Peñuelas, J., Pinol, J., Ogaya, R., and Lilella. I., Estimation of plant water content by the reflectance water index WI (R900/R970). *International Journal of Remote Sensing.* 18:2869–2875, 1997.

29. Gao, B. NDWI: A normalized difference water index for remote sensing of vegetation liquid water from space. *Remote Sensing of Environment*. 58:257–266, 1996.

30. Blackburn, G. A., Spectral indices for estimating photosynthetic pigment concentrations: a test using senescent tree leaves. *International Journal of Remote Sensing*, 19, 657– 675, 1998a.

31. Penuelas, J., Baret, F., & Filella, I., Semi-empirical indices to assess carotenoids/chlorophyll a ratio from leaf spectral reflectance. *Photosynthetica*, 31, 221– 230, 1995.

32. Blackburn, G. A., Quantifying chlorophylls and carotenoids from leaf to canopy scale: an evaluation of some hyperspectral approaches. *Remote Sensing of Environment*, 66, 273–285, 1998b.

33. Merzlyak, M.N., Gitelson, A.A., Chivkunova, O.B., and Rakitin, Y., Non-destructive optical detection of pigment changes during leaf senescence and fruit ripening, *Physiologia Plantarum*, 105: 135-141., 1999.

34. Kim, M. S., The Use of Narrow Spectral Bands for Improving Remote Sensing Estimation of Fractionally Absorbed Photosynthetically Active Radiation (fAPAR). Masters Thesis. Department of Geography, University of Maryland, College Park, MD, 1994.

35. Daughtry, C.S.T., Walthall, C.L. Kim, M.S., de Colstoun, E.B. and McMurtrey. J.E. Estimating corn leaf chlorophyll concentration from leaf and canopy reflectance. *Remote Sensing of Environment* 74:229–239, 2000.

36. Gitelson , A. A. , Keydan , G. P. and Merzlyak., M. N., Three band model for noninvasive estimation of chlorophyll, carotenoids, and anthocyanin contents in higher plant leaves. *Geophysical Research Letters* 33: L11402, 2006.

37. Sims D.A., and Gamon J.A., Relationships between leaf pigment content and spectral reflectance across a wide range of species, leaf structures and developmental stages. *Remote Sensing of Environment* 81:337-354, 2002.

38. Asner, G.P., Nepstad, D., Cardinot, G., and Ray, D., Drought stress and carbon uptake in an Amazon forest measured with spaceborne imaging spectroscopy, *Proceedings National Academy of Sciences*, 101 (16), 6039-6044, 2004.

39. Gitelson, A.A., Chivkunova, O.B., & Merzlyak, M.N., Nondestructive estimation of anthocyanins and chlorophylls in anthocyanic leaves, *American Journal of Botany*, 96(10): 1861-1868, 2009.

40. Gitelson, A.A., Merzlyak, M.N., and Chivkunova, O.B., Optical properties and non-destructive estimation of anthocyanin content in plant leaves, *Photochemistry and Photobiology*, 74(1), 38-45., 2001.

41. Van den Berg, A.K. and Perkins, T.D., Non-destructive Estimation of Anthocyanin Content in Autumn Sugar Maple Leaves, *Horticultural Science*, 40(3): 685-685, 2005.

42. Gitelson, A.A., Zur, Y., Chivkunova, O.B. and Merzlyak, M.N., Assessing Carotenoid Content in Plant Leaves with Reflectance Spectroscopy, *Photochemistry and Photobiology*, 75(3), 272-281, 2002b.

43. Rock, B.N., Vogelmann, J.E., Williams, D.L., Vogelmann, A.F., Hoshizaki, T., Detection of Forest Damage, *BioScience*, 36(7): 439, 445, 1986.

44. Serrano, L., Ustin, S.L., Roberts, D.A., Gamon, J.A., and Penuelas, J., Deriving water content of chaparral vegetation from AVIRIS data, *Remote Sensing of Environment.* 74: 570-581, 2000.

45. Sims D.A, and Gamon J.A., Estimation of vegetation water content and photosynthetic tissue area from spectral reflectance: a comparison of indices based on liquid water and chlorophyll absorption. *Remote Sensing of Environment.* 84:526-537, 2003.

46. Zygielbaum, A.I., Gitelson, A. A., Arkebauer, T.J. and Rundquist, D. C., <u>Non-destructive detection of water stress and estimation of relative water content in maize.</u> *Geophysical Research Letters* 36, L12403, doi:10.1029/2009GL038906, 2009.

47. Daughtry, C. S. T. Discriminating crop residues from soil by shortwave infrared reflectance. *Agronomy Journal* 93:125-131. 2001.

48. Serrano, L., Penuelas, J. and Ustin, S.L., Remote sensing of nitrogen and lignin in Mediterranean vegetation from AVIRIS data: Decomposing biochemical from structural signals, *Remote Sensing of Environment*, 81: 355-364, 2002.

49. Card, D.H., Peterson, D.L., Matson, P.A., and Aber, J.D., Prediction of Leaf Chemistry by the use of Visible and Near Infrared Reflectance Spectroscopy, *Remote Sensing of Environment,* 26: 123-147, 1988.

50. Daughtry, C.S.T., Hunt, E.R.Jr., Doraiswamy, P.C., and McMurtrey, III, J.E., Remote Sensing the Spatial Distribution of Crop Residues, Agronomy Journal, 864-871, 2005.

51. Milton, N.M., Eiswerth, B.A., and Ager, C.M., Effect of Phosphorus Deficiency on Spectral Reflectance and Morphology of Soybean Plants, *Remote Sensing of Environment*, 36:121-127, 1991.

52. Merton, R., and J. Huntington. Early simulation results of the ARIES-1 satellite sensor for multi-temporal vegetation research derived from AVIRIS. Available at ftp://popo.jpl.nasa.gov/pub/docs/workshops/ 99_docs/41.pdf, NASA Jet Propulsion Lab., Pasadena, CA, 1999.

53. Naidu, R.A., Perry, E.M., Pierce, F.J., and Mekuria, T., The potential of spectral reflectance technique for the detection of Grapevine leafroll-associated virus-3 in two red-berried wine grape cultivars, *Computers and Electronics in Agriculture*, 66, 38-45. 2009.

54. Gamon, J.A., Kitajima, K., Mulkey, S.S., Serrano, L., and Wright, S.J., Diverse Optical and Photosynthetic Properties in a Neotropical Dry Forest during the Dry Season: Implications for Remote Estimation of Photosynthesis, *Biotropica*, 37(4): 547-560, 2005.

55. Rahman, A.F., Gamon, J.A., Fuentes, D.A., Roberts, D.A, and Prentiss, D., Modeling spatial distributed ecosystem flux of boreal forests using hyperspectral indices from AVIRIS imagery, *Journal of Geophysical Research Atmospheres*, 106(d24), 33579-33591, 2001.

56. Roberts, D.A., Brown, K.J., Green, R., Ustin, S., and Hinckley, T., Investigating the relationship between liquid water and leaf area in clonal Populus, Proc. 7th AVIRIS Earth Science Workshop JPL 97-21, Pasadena, CA 91109, 335-344,1998.

57. Monteith, J. L. and Unsworth, M. H., Principles of Environmental Physics, 2nd ed.: London: Edward Arnold.1990.

58. Bowen, I.S., The ratio of heat losses by conduction and by evaporation from any water surface: *Physical Review*, 27, 779, 1926.

59. Roberts, D.A., Bradley, E.S., Roth, K., Eckmann, T., and Still, C., Linking Physical Geography Education and Research Through the Development of an Environmental Sensing Network and Project-based Learning, *Journal of Geoscience Education, in press*

60. Bradley, E., Still, C., and Roberts, D, Design of an Image Analysis Website for Phenological and Meteorological Monitoring. *Environmental Modelling & Software*. 25, 107-116, 2010

61. Fuentes, D., Gamon, J.A., Qiu, H-L, Sims, D., and Roberts, D., Mapping Canadian Boreal

forest vegetation using pigment and water absorption features derived from the AVIRIS

sensor, *J. Geophys. Res. Atmospheres.,* 106(D24), 33,565-33,577, 2001.